

JET PROPULSION LABORATORY**ENGINEERING MEMORANDUM****EM-3455-00-001****22 March 2000**

To Richard M. Dickinson
From Gurkirpal Singh 
Subject Characterization of Passive Dynamic Stability of a Microwave Sail

This memorandum documents the modeling, stability analysis, and simulation work related to a microwave sail being considered as a conceptual interstellar mission. The sail is constructed of carbon fiber strands few microns in thickness and 1000s of microns in length. The woven material is lightweight (density $\sim 5\text{gm/m}^2$ for material a few millimeters in thickness) and efficient in reflecting microwaves ($\sim 90\%$ reflectivity). A dynamics model of the vehicle and a model of its environment have been created. It can be used to investigate vehicle shapes offering passive dynamic stability, examine their motions, and better understand the effects of vehicle shapes and environment on vehicle stability. The intent is to characterize stability in terms of characteristic dimensions of the vehicle and, for stable configurations, determine the "region of stability"; i.e. the range of initial conditions for which the ensuing motions will remain bounded.

A stand-alone dynamics simulation environment (written in the C programming language) has been created. It can be further used to investigate vehicle motions under various initial conditions, and variations in vehicle shape and environment. It is also well suited to explore stability and natural motions of other possible vehicle configurations. In addition to providing important insights into stability characteristics of the vehicle, the work will also be helpful in validating initial experiments (1-g, vacuum) on scaled vehicle configurations.

An umbrella-like configuration, possessing an adequate center of mass – center of pressure offset, with its concave side facing the radiation source is shown to be stable in translation and rotation. Stability here implies a bounded-motion behavior. Natural damping is not modeled in this report, for material damping is not substantial enough to alter the conclusions presented here. The vehicle is modeled as a rigid body, capable of reflecting the incident radiation. Perfect reflections have been assumed. Furthermore, in order to keep the analysis manageable, multiple internal reflections of the incident radiation are not allowed. This prevents us from considering large attitude motions of the vehicle. It also prevents certain vehicle shapes from being considered in the analysis. Almost all of the work documented in this report considers a vehicle shape which has a conical "reflector" and a linear mast of appropriate length and mass to create the adequate center of mass – center of pressure offset. The mast structure coincides with the vehicle axis of symmetry. Although a conical reflector shape is considered in almost all of the work documented here, sufficient parameterization flexibility exists to model reflectors of almost any shape.

We have also proposed passive damping mechanisms (spring-dashpot arrangements) which have the potential of enhancing system damping. One such arrangement has been shown to damp system natural motions and further investigation in this direction is needed.

Distribution

Richard M. Dickinson(5 copies) (MS 238-528)
Neville I. Marzwell (MS 180-603)
Henry M. Harris (MS 301-180)
Guidance & Control Analysis Group (Section 345)

Table of Contents

1.	Introduction	1
2.	Preliminary Analysis	1
3.	Assumptions	3
4.	Vehicle Configuration and Coordinate Frame Definitions.....	4
5.	Reflector Shape Model	4
6.	The Mast Model.....	5
7.	Modeling of the Microwave Beam.....	6
8.	Vehicle Equations of Motion.....	6
9.	Conditions for Absence of Multiple-Reflections.....	7
10.	Characterization of Stability	8
11.	Domains of Stability	16
12.	Description of the Simulation Model and Environment.....	18
13.	Representative Time-Simulations.....	21
14.	Realization of Passive Damping.....	23
15.	Conclusions and Recommendations For Future Work.....	27
16.	References	28

i. Acronyms

CM	Center-of-mass
CP	Center-of-pressure
DOF	Degrees-of-freedom
NS	Neutrally-stable

ii. Notation

A	Jacobian in the neighborhood of a vehicle equilibrium state
a	Semi- major axis of the reflector base
b	Semi-minor axis of the reflector base
c_i	Reflector shape model coefficients, $i = 0, 1, 2, \dots, 4$
D	Power source offset from inertial frame origin; source location = $\{0,0,-D\}$
d	Offset between the vehicle CM and reflector CM
F	External force on the vehicle, expressed in inertial frame
G	The gravity vector in inertial coordinates; $G = \{ 0, 0, -9.807 \} \text{ m/s}^2$
g	The acceleration due to gravity, $g = 9.807 \text{ m/s}^2$
h	The height of the conical reflector
J	Vehicle inertia matrix
L	The mast length
m	Mass of the vehicle
n_x	Power index along inertial X direction
n_y	Power index along inertial Y direction
P_t	Transmitted power
q	Vehicle attitude (quaternion)
R	Reflector radius (variable for elliptical bases)
r_c	Inertial position of vehicle CM
T	External torque on the vehicle, expressed in body frame
v_c	Inertial velocity of vehicle CM
w	Span of a circular cone reflector ($a = b = R = \frac{1}{2} w$)
\bar{x}	Vehicle state ($= \{r_c, q, v_c, \omega\}$)
x_c	X_I coordinate of the vehicle CM ($\equiv r_c(1)$)
y_c	Y_I coordinate of the vehicle CM ($\equiv r_c(2)$)
z_c	Z_I coordinate of the vehicle CM ($\equiv r_c(3)$)
ρ	Power density (watts/meters ²)
ω_c	Vehicle angular rate
Ω	Vehicle spin rate (i.e. the rate about z axis)
•	Scalar product
×	Vector product
⊗	Quaternion multiplication
(.) ^T	Transposition of the vector or matrix argument

1. Introduction

The idea of converting electromagnetic energy into mechanical energy is not new. Publications dating back to 1962 have made such propositions¹. The proposal to use a microwave beam to propel an interstellar spacecraft forces one to address several important issues from the standpoint of control. The idea is to generate the needed thrust by reflecting an incident microwave beam. The microwave generator may be on earth, in an earth orbit, on another terrestrial body, or in an orbit around a terrestrial body.

In order for such a propulsive approach to be viable, it will be important for the spacecraft to possess passive stability, i.e. it must have the ability to "adhere" to the microwave beam. It will simply be not practical for the spacecraft to carry the resources needed for active propulsive and attitude control for missions lasting several decades. Passive stability can be realized by constructing a vehicle of appropriate shape and mass distribution. We have shown that certain umbrella-like configurations possessing appropriate center of mass - center of pressure offsets, with their concave sides facing the radiation source are neutrally stable in translation and rotation. "Stability" here means a bounded-motion behavior. Furthermore, mission design will dictate possibly continuous steering of the beam. The craft therefore shall also have the ability to "track" small and possibly continuous changes in the direction of the beam.

2. Preliminary Analysis

Significant analysis effort was spent in the initial phase of this work to explore promising shapes and mass distributions. This effort did not consider the most general problem, rather a simplification of it. It considered planar motions of the vehicle. It was felt that, once an appropriate shape for the planar motion case had been found, it should be possible to generalize it to the three-dimensional case. By the same argument, if the vehicle shape were found to be unstable in the planar motion case, it would certainly not be stable in three dimensions. A number of configurations were ruled-out as a result. The one offering the most promise was an umbrella-like structure with an adequate center of mass - center of pressure offset, with the concave side facing the source of the radiation.

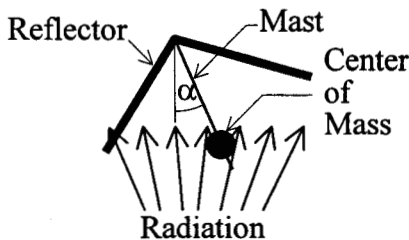


Figure 1. A Stable Configuration in the Planar Case

A representative planar displacement (translation in the plane of the paper and rotation α) in the radiation field is shown in Figure 1. It also identifies the components of the vehicle we shall be referring to several times in this report: the wedge-shaped *reflector* and the *mast*. The reflector is made out of a lightweight ($\sim 5\text{gm/m}^2$) carbon fiber material. The spacecraft will not need a mast, if it were not for the explicit need to attain passive attitude stability. The mast is rigidly attached to the reflector, in other words no articulation is allowed at the point of attachment (we will relax this restriction later on). The mast does not present a significant cross section to the incident radiation, and is therefore assumed to not reflect or absorb any radiation. The light-weight reflector is where nearly all of the reflections take place. This locates the vehicle center of

pressure (CP) in the vicinity of the reflector. Adequate CP-center of mass (CM) offset can be obtained by adding some “ballast” at the appropriate location on the mast. Almost all of the vehicle mass is therefore at or near this added mass. In actual applications the ballast may take the form of the spacecraft bus. Analysis of the simplified model allows us to draw the following general conclusions from the standpoint of attaining passive dynamic stability:

- i) The beam reflecting area of the vehicle (the reflector in Figure 1) must be located aft of the vehicle center of mass for rotational stability, and
- ii) the reflector must be of an appropriate concave shape such that the concave side faces the radiation source. This is apparently a necessary condition for translation stability. This is made possible by a near-gaussian beam-power density variation, which decreases with the translation away from the center of the beam. A more precise model of this variation will be provided later on (Section 6). Figure 1a depicts how the particular reflector shape and beam power density variations, together, offer the needed lateral dynamic stability. At a fixed range from the power source, the beam

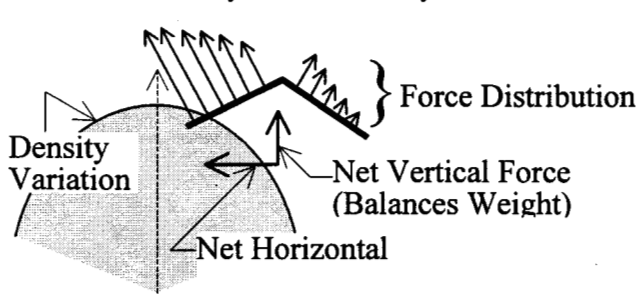


Figure 1a: Beam Interactions with Vehicle Shape to Create a Restoring Force

density or flux varies as $\sim \text{Cos}(\theta)^n$ where θ is the angle between the power source \rightarrow location vector and the beam axis and n is the power index. The flux therefore decreases with increasing θ , and the flux gradient depends on n . The conical shape and the particular density pattern together provide lateral or translational stability. The force at a particular

reflector location is approximately aligned with the local surface normal. Also, the force magnitude on reflector locations further away from the beam-axis is smaller. The net force on the vehicle is obtained by integrating elemental forces over the entire reflecting surface. The elemental force can be resolved into a vertical component and a horizontal component. The integration of all vertical components provides the needed lift to counter the effects of gravity and all horizontal forces can be seen to add up to a net force towards the beam axis, providing the vehicle with the needed restoring force.

In the aftermath of these early conclusions, generalizations were made to the three-dimensional case and subsequent analyses focused on configurations with a conical reflector, for it can be parameterized with the smallest number of parameters. Henceforth, most of the work will consider a vehicle with a conical reflector and a linear mast of appropriate length and mass running along the vehicle axis of symmetry. Sufficient parameterization flexibility exists in the model however to allow arbitrarily shaped reflectors. In the sequel, we will also consider variations of this model where relative motions between the reflector and the mast are permitted.

3. Assumptions

- a) The spacecraft possesses a large reflecting cross-section. The vehicle mass distribution is such that the CM is located between the reflector and the radiation source.
- b) The reflector is modeled as a rigid body. In reality the reflector material will tend to warp in the incident radiation field and it may also have dynamics / thermal-gradients induced ripples or distortions. Such static and dynamic effects have been ignored here. It is felt that the light-weight carbon fiber material used to construct the reflector will have to be strengthened and rigidified to minimize warping, tears as a result of dynamic stresses and meteoroidal impacts. Ignorance of these non-rigid effects is therefore not a strong assumption.
- c) The mast neither absorbs nor reflects any of the incident radiation. The smallness of the mast structure cross-section makes this an appropriate assumption.
- d) There are no internal reflections, i.e. the incident radiation is allowed to be reflected only once by the reflector structure. This assumption places limits on allowable attitude excursions and reflector shapes and size. These assumptions, however, are not hard to satisfy and conditions will be presented later on to ensure this. It is possible to include multiple reflections in the analysis, but at the cost of significant additional modeling complexity. Future extensions of this work may consider modeling of these effects.
- e) The reflector cross section orthogonal to the incoming radiation is elliptical in general. This is consistent with the shapes under consideration at this time.
- f) The reflector shape resembles an elliptical cone (elliptical base, as noted in (e)). Justifications for this assumption were provided earlier. The primary reason for this *restriction* is the number of parameters needed to model such a surface. A smaller parameter set helps reduce the parameter space to be explored later on for stability analyses. We point out, once again, that the reflector model in the analysis allows arbitrary shapes.
- g) The vehicle is operating in a uniform 1-g environment. The removal of this assumption will not alter the conclusions of this report. The presence of a 1-g field simply increases the power required to stabilize the vehicle.
- h) There are no aerodynamic influences. This also holds true for the experiments to be carried out in vacuum.
- i) Beam power density varies in the inverse square proportion to the separation from the source (refer to Section 6 for specific density model used in the analysis).
- j) The radiation source is modeled as a point source.
- h) Perfect reflections take place at the reflector surface. Nearly 90% reflectivity of the material being considered for this application makes this a reasonable assumption as well.

4. Vehicle Configuration and Coordinate Frame Definitions

Two coordinate frame definitions are needed here (see Figure 2), these are: the inertial frame and the body frame. The body frame $\{x_b, y_b, z_b\}$ is attached to the vehicle CM and moves with it. The body z-axis is aligned with the mast axis. The inertial frame $\{X_I, Y_I, Z_I\}$ is such that the gravity acts along the $-Z_I$ direction. The microwave beam point

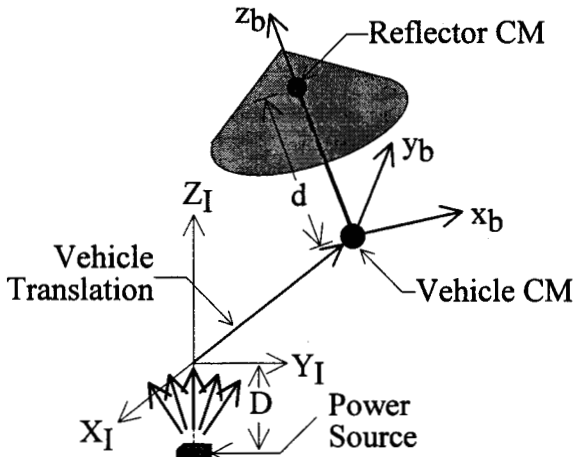


Figure 2. Spacecraft Configuration and Coordinate Frame Definitions

source is also located on the Z_I axis at inertial coordinates $\{0, 0, -D\}$ ($D > 0$). The microwave beam is radiating in the $+Z_I$ direction such that maximum intensity direction coincides with the $+Z_I$ axis. The quantity d ($d > 0$) specifies the offset between the vehicle CM and the reflector CM. In our analysis, the vehicle initial conditions will be such that the vehicle CM is located at or near $\{0, 0, -d\}$ in inertial coordinates. Therefore the separation between the power source and the reflector CM will be approximately D in almost all cases. The vehicle possesses three rotational and three translational degrees of freedom.

5. Reflector Shape Model

Any reflector cross section orthogonal to the mast is an ellipse, in general. The reflector surface is generated as a surface of revolution, by rotating a parameterized curve about the body z-axis. The following fourth order polynomial parameterization is used:

$$f(r/R) = c_0 + c_1 (r/R) + c_2 (r/R)^2 + c_3 (r/R)^3 + c_4 (r/R)^4 \quad (1)$$

where c_i , $i = 0, 1, 2, \dots, 4$, are some shape constants. For example, a conical reflector is realized when $(c_0, c_1) \neq 0$, and $(c_2, c_3, c_4) = 0$; $c_1 < 0$ results in the desirable concave-facing-down shape. Figure 3 further depicts this parameterization. A reflector-fixed cylindrical coordinate frame $\{r, \psi, z (\equiv z_b')\}$ may be defined such that at each ψ station $Max(r) = R$, where R is a function of ψ and the reflector base semi-major and semi-minor axes (a, b respectively). The elliptical base shape is characterized as:

$$R^2 \{ (\cos\psi/a)^2 + (\sin\psi/b)^2 \} = 1, \quad (2)$$

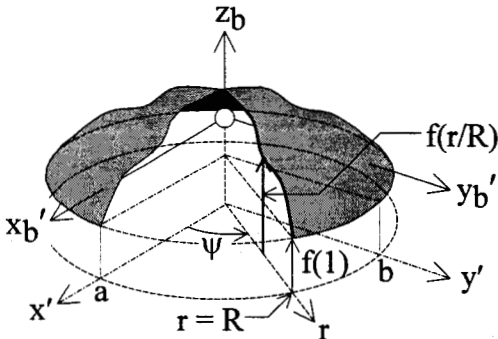


Figure 3. Reflector Shape Model

which allows R to be expressed as a function of ψ, a, b . The shape characterization proceeds as follows. At each (r, ψ) location, use (2) to compute R and, subsequently, equation (1) to locate the z component ($\equiv f(r/R)$) or the "height" of the reflector. This parameterization is quite general and more complex shapes may be modeled by including additional terms in the power series (1). The only restriction on

reflector shape here is the assumption regarding the elliptical base. A circular base is realized by setting $a = b = \frac{1}{2}$ reflector-span ($= w/2$). A sampling of possible reflector shapes using this parameterization is shown in Figure 4. The two shapes at the top have a circular base (0.5 meter radius) and the other two have an elliptical cross-section ($a = 0.5$ m, $b = 0.8$ m). The shape at the top-left is a circular cone. The related coefficient values ($c_0, c_1, c_2, c_3, c_4, a, b$) are shown at the top of each shape. The coordinate frame used for these depictions is the $\{x', y', z_b\}$ frame of Figure 3. Clearly, a wide variety of shapes can be modeled by using the chosen parameterization (1).

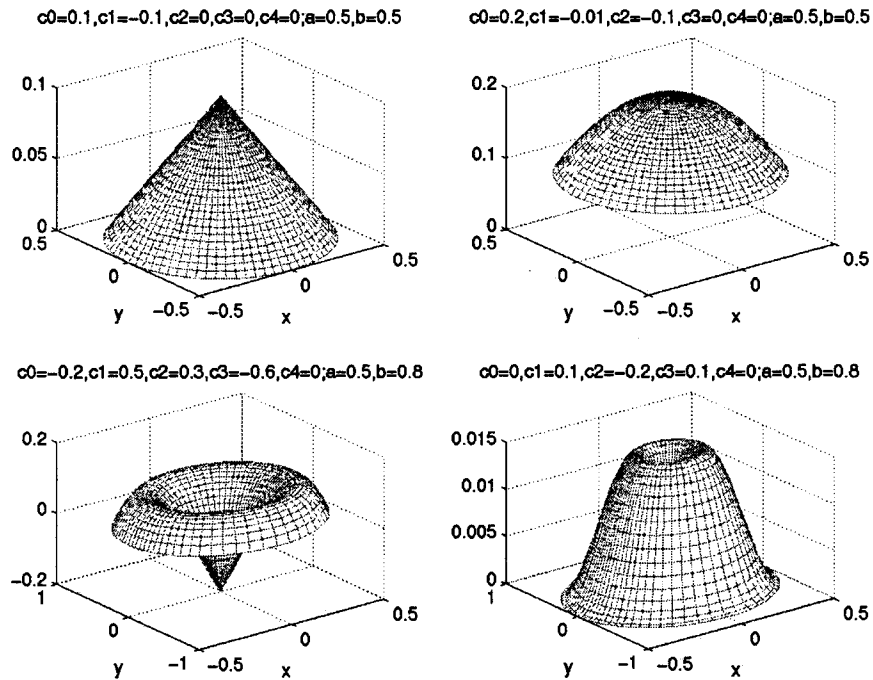


Figure 4. A Sampling of Possible Reflector Shapes

6. The Mast Model

No definitive mast structure models are available at this time. Therefore additional assumptions regarding materials and dimensions were made so that unrealizable mass properties are not used in the analysis. It should be pointed out that these assumptions are not critical to the analysis. These are made strictly from the standpoint of physical realizability. The mast is assumed to be a system of two rigidly connected bodies: a spherical Lead mass and a long slender hollow Titanium tube (a hollow tube for it will have a greater bending stiffness). The tube is a cylinder of 0.5 mm radius and 0.2 mm thickness and the spherical ball is 5 mm in radius. The ball is located at one end of the tube (the "mast") and the other end is assumed attached to the reflector structure at the reflector CM. The length of the tubular structure (L) is a parameter which can be varied in order to realize the desired CM-CP offset.

7. Modeling of the Microwave Beam

Per the convention adopted in Figure 2, the microwave source is fixed in the inertial frame at $\{0, 0, -D\}$, $D > 0$. The source is modeled as a point source. The power density drops off in inverse square proportion to the distance. A rectangular wave-guide photon beamer will be used in the initial experiments². For such a wave-guide, the energy density (units: watts/m²) at location $\{x, y, z\}$ in inertial coordinates is well approximated by the following equation (see Figure 5):

$$\rho = P_t \{ (\cos\phi)^2 (\cos\theta)^{n_x} + (\sin\phi)^2 (\sin\theta)^{n_y} \} / (4 \pi s^2), s \geq 0, \quad (3)$$

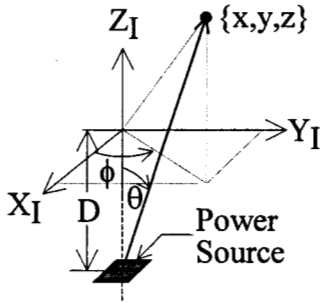


Figure 5. Power Density Model Definitions

where

P_t is the transmitted power (watts)

s is the range from the source,
 $= \{ x^2 + y^2 + (z+D)^2 \}^{1/2}$

θ is the angle between the source \rightarrow location vector and $+Z_I$, $= \tan^{-1} \{ (x^2 + y^2)^{1/2} / (z+D) \}$

ϕ is the "clock" angle (measured from $+X_I$) of the location, $= \tan^{-1}(y, x)$

n_x, n_y are tunable indices, referred to as the *power indices* in the sequel, which depend on the dimensions of the wave-guide

8. Vehicle Equations of Motion

The vehicle possesses six degrees of freedom. A general vehicle displacement can be expressed as a translation of the vehicle CM and a general rotation of the body frame with respect to the inertial frame. Attitude quaternion q specifies the body-frame orientation in inertial coordinates. Let vector $r_c = \{x_c, y_c, z_c\}$ denote the inertial coordinates of the vehicle CM. A general displacement of the craft is therefore expressed as the 7-vector $\{q, r_c\}$. Vehicle's equations of motion, under the assumption that it is a rigid body, are particularly simple in this case:

$$\dot{r}_c = v_c, \quad (4)$$

$$\dot{q} = \frac{1}{2} \omega \otimes q, \quad (5)$$

$$\dot{v}_c = F / m + G, \quad (6)$$

$$\dot{\omega} = J^{-1} [-\omega \times J\omega + T], \quad (7)$$

where v_c is the inertial velocity of the vehicle CM, ω is the angular rate vector in body coordinates, \otimes is the quaternion multiplication operation, J is the vehicle moment of inertia, m is the vehicle mass, G is gravity vector ($G = \{0, 0, -9.807\}$ m/s² here), F is the radiation-induced inertial force on the vehicle, and T is the radiation-induced body torque on the vehicle, about the vehicle CM. Note that the computation of F and T requires evaluation of area integrals over the entire reflecting surface. It is impossible to carry out these evaluations analytically. Consequently these integrals are approximated by discrete summations. To facilitate these discrete summations, the reflector is divided into a finite

number of small uniformly distributed elements. The only restriction imposed on these elements is that they have the same area when projected onto the x_b - y_b plane. Define the following variables:

r_{eb}	Vehicle CM→element location vector in the body-frame
r_{eI}	Reflector element location vector in inertial-frame: $r_{eI} = \{x_{eI}, y_{eI}, z_{eI}\} = r_c + q^* \otimes r_{eb} \otimes q$
\hat{n}_{eb}	Reflector unit normal in the body-frame at location r_{eb}
dA	Element area when projected onto the x_b - y_b plane
dA_e	Actual element area, $= dA / \hat{n}_{eb}(3) $. This follows since the third element of the vector \hat{n}_{eb} is the Cosine of the \hat{n}_{eb} - z_b angle.
dF_b	Radiation-induced element force in body-frame
ρ_e	Power density at the element location. It is a nonlinear function of element location r_{eb} , vehicle attitude q , and displacement r_c .
ψ_e	The angle between the element local normal and direction to the source

The components $\{x_{eI}, y_{eI}, z_{eI}\}$ of r_{eI} are used in (3) to compute ρ_e , the power density at the element inertial location. The inertial vector from the radiation source to the element location is $\{x_{eI}, y_{eI}, z_{eI} + D\}$. The *cosine* of the angle between the element local normal and the direction of incident radiation is hence:

$$\text{Cos}\psi_e = \text{Unit}(\{x_{eI}, y_{eI}, z_{eI} + D\}) \bullet q^* \otimes \hat{n}_{eb} \otimes q \quad (8)$$

The elemental force vector, assuming perfect reflection, can be expressed as:

$$dF_b = 2 dA_e \rho_e \text{Cos}\psi_e^2 \hat{n}_{eb} = 2 dA \rho_e \text{Cos}\psi_e^2 \hat{n}_{eb} / | \hat{n}_{eb}(3) |. \quad (9)$$

Hence:

$$F = q^* \otimes \{ \iint_{\text{Reflector}} dF_b \} \otimes q, \quad (10)$$

$$T = \iint_{\text{Reflector}} (r_{eb} \times dF_b). \quad (11)$$

As noted earlier, a discrete sum (double summation) is used to approximate the area integrals involved in (10), (11).

9. Conditions for Absence of Multiple-Reflections

The analysis/simulation results presented here make the assumption that the incident radiation is reflected only once by the reflector structure. The absence of multiple reflections is the principal assumption of the work. It is possible to model these effects in the numerical simulation but at a significant additional run-time cost. The models will have to employ techniques similar to ray-tracing methods to detect multiple reflection conditions and this must be carried out at each reflector element location. Although multiple beam reflections will tend to lower the power required to levitate a structure of a given mass, the implications for vehicle stability are not immediately obvious. This is indeed one aspect of the model where significant fidelity improvement is possible.

It is difficult, in general, to analytically state conditions for which multiple reflections will not take place. The condition will, in general, depend on vehicle shape, size, and position and orientation with respect to the beam source. We shall make some reasonable

assumptions under which a simple statement of this condition becomes possible. Restricting ourselves to the planar motion case (no loss of generality) and consideration

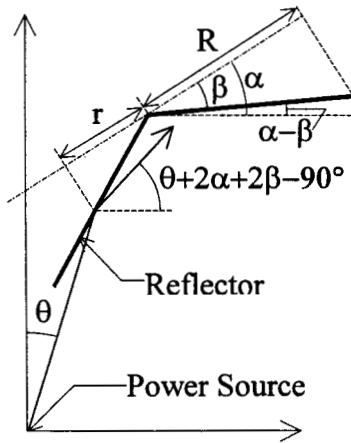


Figure 6. Multiple Reflections

of only the conical reflectors, we can state the following condition, which implies that the *slope* of the reflected ray be smaller than the *slope* of the intended reflecting surface (the surface on the right in Figure 6): $\theta + 2\alpha + 2\beta - 90^\circ < \alpha - \beta$, where α is the vehicle attitude, β is the complement of the reflector half-cone angle, and θ is the angle with the power source. This condition must hold for all applicable θ values (i.e. for all r values: $0 < r \leq R$), which changes with the location on the reflector. Alternatively, the following must be satisfied:

$$\beta < 30^\circ - (\theta + \alpha)/3. \quad (12)$$

Angle θ depends on the position of the vehicle. For small attitude and lateral deviations of the vehicle (i.e. small compared with β), it is possible to state (12) as the following upper bound on reflector height for absence of multiple reflections in the case of conical reflectors:

$$h < 0.577 b, \quad (13)$$

where h is the cone height and b is it's semi-minor axis. A more realistic and tighter bound on the height of the reflector must also take into account vehicle attitude and location with respect to the power source. While (13) serves as a rough verification of absence of multiple reflections from the reflector structure, it is more appropriate to implement this check numerically, i.e. implementation of (12) where actual θ and α values are used in the determination of maximum permissible β value.

10. Characterization of Stability

Let vector $\bar{x} = \{r_c, q, v_c, \omega\}$ denote the vehicle state. The equations of motion (4-7) can be compactly written as the following nonlinear vector differential equation:

$$\dot{\bar{x}} = \mathcal{F}(\bar{x}), \quad (14)$$

where $\mathcal{F}(\bar{x})$ is a nonlinear vector function (the right hand sides of eqns. (4-7)) of vehicle states, shape and intensity parameters. It is not hard to show that $\mathcal{F}(\bar{x}) \equiv 0$ when $\bar{x} = \bar{x}_0 = \{r_c = (0,0,z_{eq}), q = (0,0,0,1), v_c = (0,0,0), \omega = (0,0,0)\}$, i.e. the vehicle will be in a state of equilibrium when it is not rotating or translating and is located directly above the radiation source at an arbitrary z offset (z_{eq}) with $z_b \parallel z_l$. This assumes that sufficient power is available to keep it levitating at $z_c = z_{eq}$, i.e. $F(\bar{x} = \bar{x}_0) = mG$. Note that the circular symmetry at this attitude assures that $T \equiv \{0,0,0\}$. Let \bar{x}_0 be the "null" state of the vehicle. It is clearly an equilibrium. There are no other equilibrium for the vehicle shapes and the radiation fields under consideration. The question ... "for what vehicle configurations is the null state a "stable" equilibrium ?", will be addressed next. By "stability" we really mean neutral stability here (bounded motion behavior – the best we can hope for in the absence of natural damping). Note that the equations of motion (4-7)

are highly nonlinear on account of dependence of T and F on vehicle position and attitude. The question of stability can be addressed by linearizing (14) in the neighborhood of the null state and solving the associated eigen-value problem. Numerical means are resorted to for linearization and a matrix, linear, first order differential equation is obtained:

$$\delta \dot{\bar{x}} = \left[\frac{\partial \mathcal{F}}{\partial \bar{x}} \right]_{(\bar{x} = \bar{x}_0)} \delta \bar{x} = A \delta \bar{x}, \quad (15)$$

where $\delta \bar{x}$ are “small” perturbations from the null state and the matrix A is the Jacobian evaluated at the null state. The stability of the system of equations (4-7) for small motions in the neighborhood of \bar{x}_0 depends on the eigenvalues of matrix A, which may be real and / or complex conjugate pairs. Eigenvalues of A may be written, in general, as $\lambda_i = u_i + j v_i$. It is not reasonable here to expect $u_i < 0$ for some eigenvalues of a stable system (lack of natural damping). The best we can hope for is a neutrally-stable vehicle for which all eigenvalues must lie on the imaginary axis in the complex plane, meaning that $u_i = 0$ for all roots is the condition for absence of instability.

The vehicle possesses six dynamic modes (six degrees of freedom). One is a rigid body mode (zero frequency) which tends to rotate the vehicle about the Z axis. The remaining five are the five fundamental oscillatory modes. The first is a “bouncing” or a “hopping” mode, which makes the vehicle translate up and down along the inertial Z axis, it is always neutrally stable. The other four are combinations of attitude and translation motions in the $Y_I Z_I$ - and the $X_I Z_I$ -planes. These modes may be looked upon as combinations of “pendulum” and side-to-side “yo-yo” modes. It is the stability of these four modes which determines the neutral stability of the vehicle.

We shall assume that the z location of the null state is such that $z_{eq} = -d$. D is then exactly the offset between the reflector CM and the power source. We now proceed to characterize vehicle neutral stability as a function of shape and radiation source parameters, which, assuming it to have a circular base reflector, are:

- D the separation between reflector CM and the power source,
- L the mast length ($\approx d$, the reflector CM - vehicle CM separation)
- w the span of the circular-base reflector,
- n_x, n_y the power indices,
- h the reflector height $h (= |c_1|)$,
- Ω the vehicle spin rate about z_b (i.e. $\omega = \{ 0, 0, \Omega \}$)

Note that later on we shall also consider the effect of vehicle z-axis spin on stability. It is therefore also treated as a parameter to be varied here. Let \mathcal{P} define the parameter set, i.e. $\mathcal{P} = \{D, L, w, n_x, n_y, h, \Omega\}$. Only one element of this set is varied at a time. In each instance the transmitted power is adjusted so that the net upward force cancels the gravity (levitation condition). A neutrally stable configuration was found to exist for the parameter set $\mathcal{P}^* = \{D = 0.4 \text{ m}, L = 0.33 \text{ m}, w = 0.22 \text{ m}, n_x = 2.5, n_y = 2.5, h = 0.06 \text{ m}, \Omega = 0^\circ/\text{s}\}$. Note that although other neutrally-stable parameter sets exist, the discussion to follow will be restricted mostly to parameter variations in the neighborhood of \mathcal{P}^* . Also note that for this parameter set, multiple reflection condition is satisfied for small attitude and position excursions. The condition requires that the reflector height h be smaller than 6.4 cm for a circular reflector span of 22 cm.

10.1 Variation in Circular Reflector Span w

All elements of \mathcal{P}^* , except w , are fixed at the values noted above and the span w is varied in the interval (0.20, 0.26) m. The variation in u_i (the real part of the eigenvalues of A) with w , the span, are shown below (the Figure on the left). The fixed elements of the parameter set are noted at the top in the Figure. For the parameter set and the range of w values under consideration, the resulting configurations are neutrally stable only when span w lies in the 0.211 m \rightarrow 0.227 m range (real parts of all eigenvalues are zero in this range). The range satisfies the no-multiple-reflection constraint: $w > 0.208$ m ($h = 6$ cm).

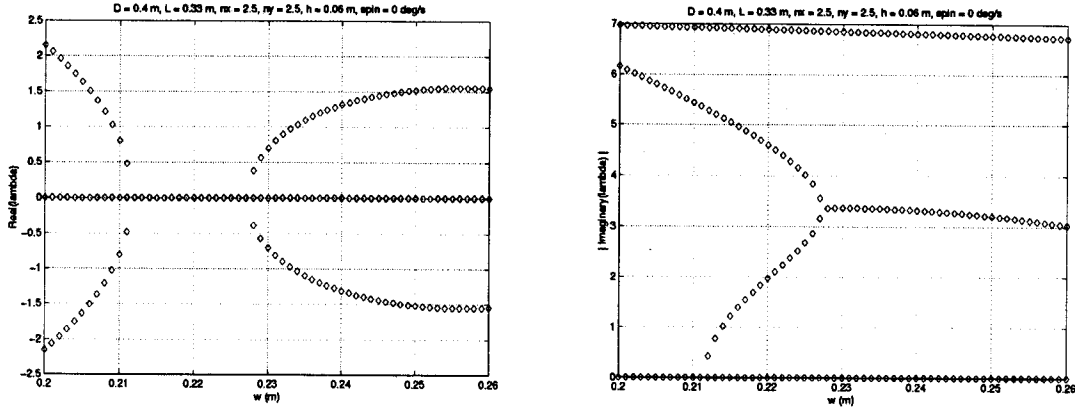


Figure 7. Variation in Eigenvalues Real and Imaginary Parts with Span (w)

Note that for NS configurations the imaginary part of the eigenvalues, i.e. $|v_i|$ are the associated oscillation frequencies (units: rad/s). The plot on the right in Figure 7 depicts the $|v_i|$ vs. w variation. The frequency which appears to change little with w is the hopping mode frequency (~ 7 rad/s or approximately 1.1 hz). The others (< 5 rad/s in the NS w range) belong to the yoyo-pendulum modes. The zero frequency is the rigid-body mode denoting a pure rotation about the z_b axis. It is possible to analytically approximate the hopping mode frequency for nearly flat reflectors and circular beams. The following approximation can be made:

$$\omega_{\text{hop}} \approx \left[\frac{(g/D) (n+2) \hat{w}^2 (1+\hat{w}^2)^{-n/2-1}}{\{\hat{w}^2 + [1 - (1+\hat{w}^2)^{-n/2}]\}} \right]^{1/2}, \quad (16)$$

where $\hat{w} = w / (2 D)$, n is the power index, g is the acceleration due to gravity, and we have assumed that sufficient power is applied to make the vehicle levitate at distance D away from the source (i.e. at the reflector-source separation of D). In the example here, $D = 0.4$ m, $n = 2.5$. The estimate of the hopping mode frequency at $w = 0.22$ m ($\hat{w} = 0.275$) is found to be 6.6 rad/s, in good agreement with the numerical result.

Note that the first plot in Figure 7 indicates that the real parts of the unstable eigenvalues are increasing at a smaller rate as $w \rightarrow 0.26$ m, suggesting that other NS configurations perhaps exist as w is increased further. A larger w range (0.20 m, 0.36 m) was therefore considered next, and indeed another very narrow NS w set was found at (0.283, 0.285) m. The related plots appear below in Figure 8. Note again the insensitivity of the hopping mode to variations in w . It is noteworthy that the configurations remain unstable for w values outside the (0.2, 0.36) m interval. Therefore there appear to be only two distinct ranges of the parameter w for which NS configurations will exist.

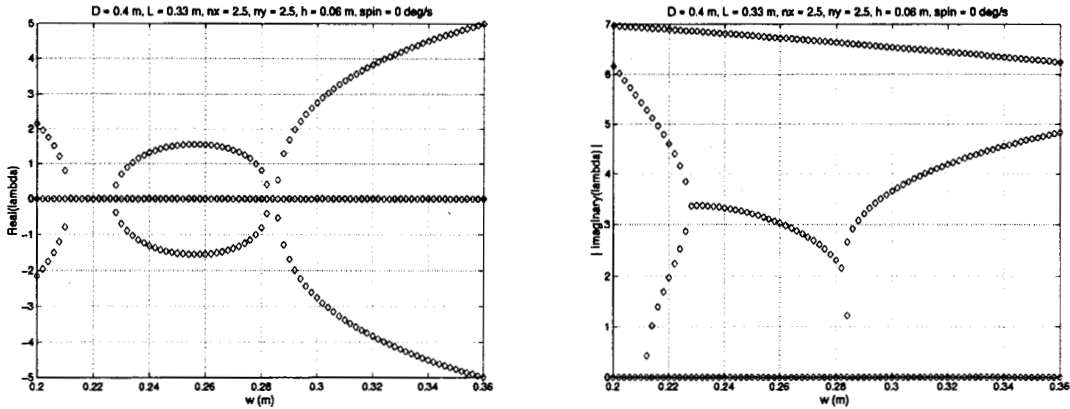


Figure 8. Variation in Eigenvalues Real and Imaginary Parts with Span (w)

The stability tendency noted here, unstable as w approaches large and small values, is not unexpected. Recall that the vehicle derives rotational stability from a favorable CP-CM offset and it derives translational stability from its shape and environment, i.e. the variation in beam density (see Figure 1a). There are two contributors to the force at any location: the flux which decreases as the angle from the beam axis is increased, and the incidence angle which is the angle between the incident radiation and the local surface normal. It is the square of the Cosine of this angle which matters and a smaller incidence results in a greater force. Note that, as w is increased, the configuration tends towards a flat plate which is known to be unstable. At the other extreme are the smaller w values which, although give a more efficient configuration, meaning a greater lateral force component, also tend to decrease the incidence angle on the outboard element, which counteracts the benefits of a favorable flux gradient. It is therefore natural to expect a smaller bound on w below which a NS vehicle configuration will not exist.

There appear to be 3 modes (Figure 8, right) for NS configurations. There are in fact 5 oscillatory modes here: one hopping mode and two repeated yoyo-pendulum modes. The repeated pair is a consequence of symmetry, i.e. symmetric vehicle and / or beam configurations. To observe this, consider the same parameter set with the difference that $n_x = 2.5$, $n_y = 2.2$. The related eigenvalue plots appear below in Figure 8a. Note that the

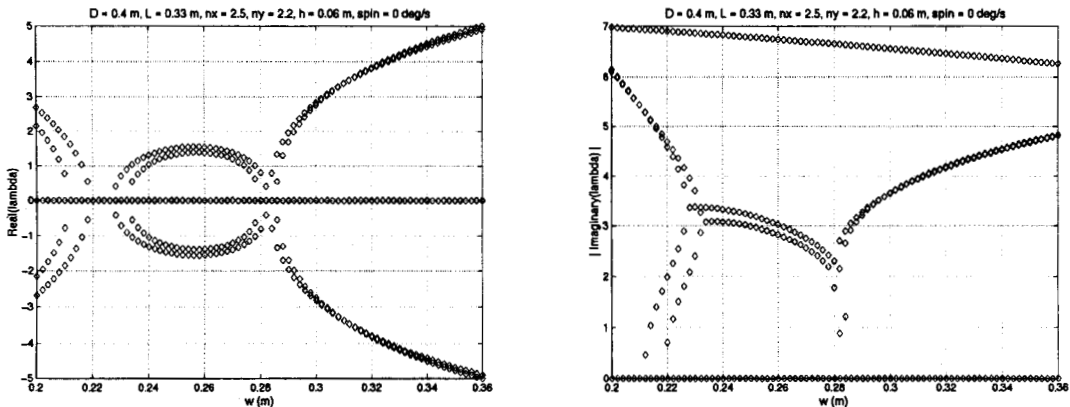


Figure 8a. Variation in Eigenvalues Real and Imaginary Parts with Span (w), $n_x \neq n_y$

NS w ranges have shrunk somewhat to $\sim(0.219, 0.227)$ m and $\sim(0.2826, 0.2831)$ m. Also, one of the repeated pairs of roots appears different now (lack of circular beam symmetry) and the five distinct frequencies are clearly evident in the NS w range (the Figure on the right).

We consider two more variations of the original parameter set used in Figure 8: the first where the height of the cone is reduced to 0.05 meters and the other where it is increased to 0.07 meters. The stability region variations for these appear side by side below in Figure 8b. The width of the stable w set does not appear to change appreciably, but its location does, a bigger span is required, in general, for neutral stability for a taller conical reflector (approximate preservation of reflector aspect ratio). Note that the NS w range in the plot on the left in Figure 8b starts at $w = 0.195$ m.

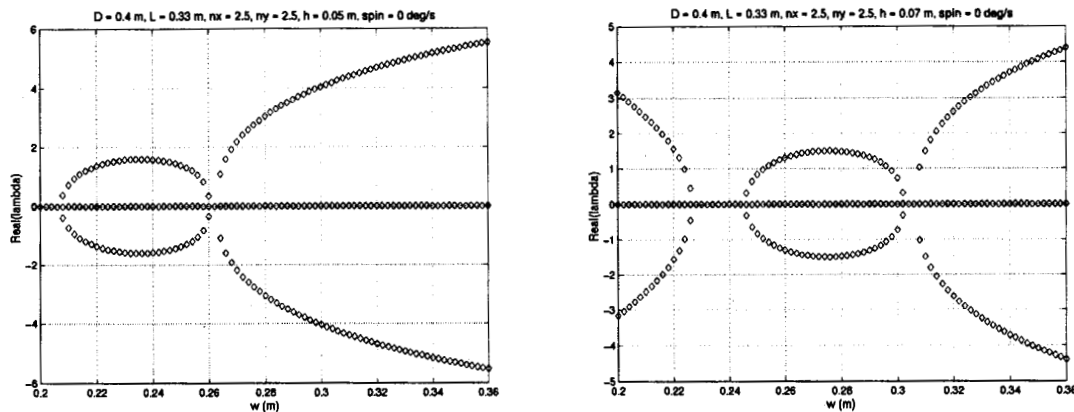


Figure 8b. Variations in Stability Regimes for $h = 0.05$ m (Left), and $h = 0.07$ m (Right)

10.2 Variation in Reflector – Source Separation D ($0.3 \text{ m} \leq D \leq 0.5 \text{ m}$)

The nominal parameter set in this case is chosen to be $\mathcal{P}^* = \{D, L = 0.33 \text{ m}, w = 0.22 \text{ m}, n_x = 2.5, n_y = 2.5, h = 0.06 \text{ m}, \Omega = 0^\circ/\text{s}\}$. Note that D is the parameter to be varied in this case. The variation in u_i and $|v_i|$ with D is shown in Figure 9. The system is neutrally-stable when D lies in the $(0.38, 0.42)$ m range. The hopping mode frequency is still around 1 hz, but shows a sharper decline (varies approximately as $D^{-1/2}$ per eqn.(16)). The other frequencies display the tendencies noted before.

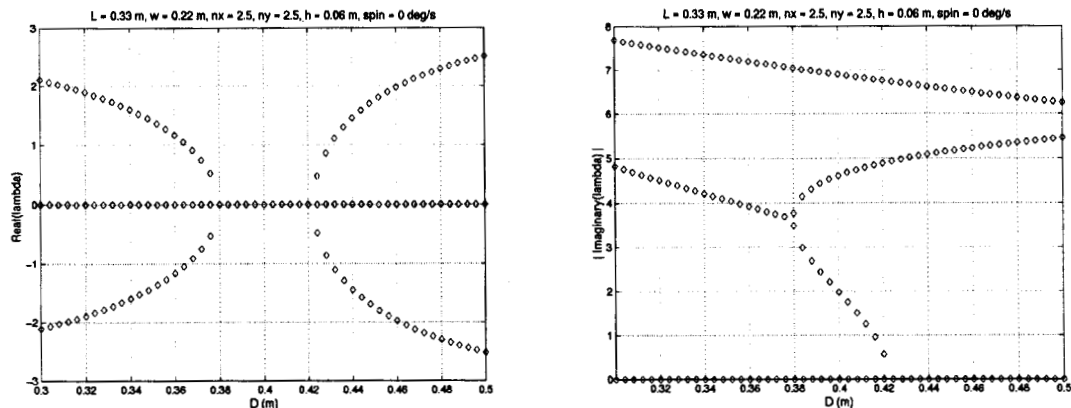


Figure 9. Variation in Neutral Stability and Frequencies with Distance from Source D

The variations noted above are, again, expected. A lower bound on D exists because a lowering of D , although it sharpens the flux gradient, also reduces the incidence angle on the outboard elements. A lower bound on D will therefore exist where the effects of reduced incidence angles will overcome the gradient influence. An upper bound on D (the vehicle size is not varied in this instance) exists since the flux gradient across the vehicle span is likely to be insufficient for neutral stability at greater separations.

10.3 Variation in Mast Length L ($L: 0.2 \text{ m} \leq L \leq 0.5 \text{ m}$)

The nominal parameter set in this case is chosen to be $\mathcal{P}^* = \{D = 0.4 \text{ m}, L, w = 0.22 \text{ m}, n_x = n_y = 2.5, h = 0.06 \text{ m}, \Omega = 0^\circ/\text{s}\}$, L is the parameter to be varied. The configurations are NS when for mast lengths in the $(0.28, 0.42)$ m range. The related plots are shown below in Figure 10. Note that for $L > 0.4 \text{ m}$, the ball at the end of the 0.4 m mast will actually lie below the wave guide opening.

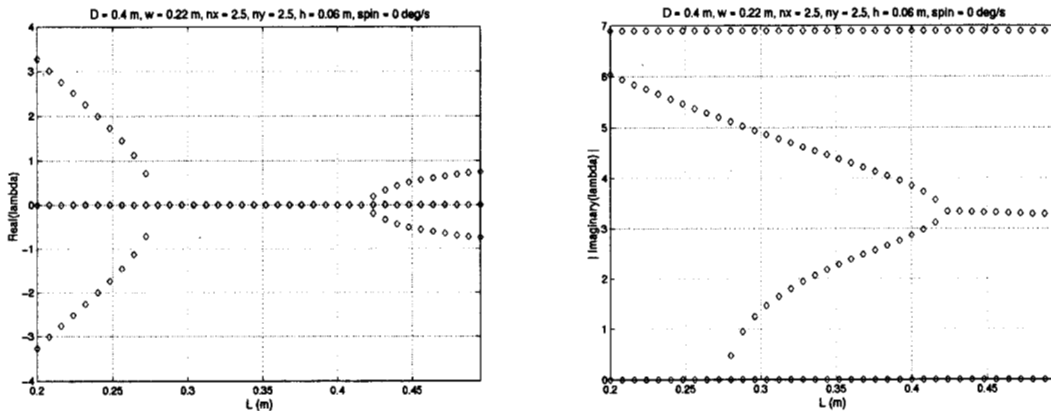


Figure 10. Variation in Neutral Stability with Mast Length L

10.4 Variation in Power Indices, n_x, n_y ($n_x = n_y = n: 1.5 \leq n \leq 4$)

A circular beam ($n_x = n_y = n$) is considered and the nominal parameter set in this case is: $\mathcal{P}^* = \{D = 0.4 \text{ m}, L = 0.33 \text{ m}, w = 0.22 \text{ m}, n_x = n_y = n, h = 0.06 \text{ m}, \Omega = 0^\circ/\text{s}\}$. The parameter n , the power-index, is to be varied in this case in the interval $(1.5, 4)$. The variations in u_i and $|v_i|$ with n ($= n_x = n_y$) are shown in Figure 11. The system is found

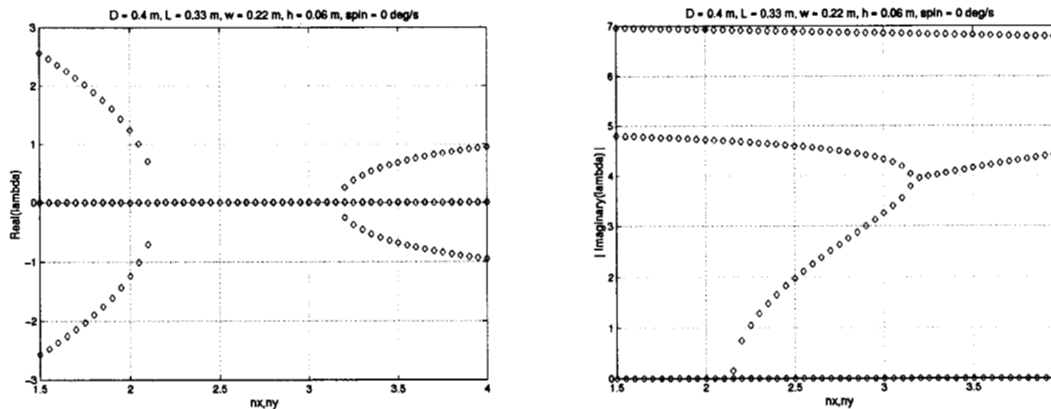


Figure 11. Variation in Neutral Stability with Power Index

to be neutrally-stable when, for a circular beam, n lies in the (2.15, 3.15) range.

10.5 Variation in Reflector Height h

The nominal parameter set $\mathcal{P}^* = \{D = 0.4 \text{ m}, L = 0.33 \text{ m}, w = 0.22 \text{ m}, n_x = n_y = 2.5, h, \Omega = 0^\circ/\text{s}\}$, where h is the varied parameter to be varied in the interval (4, 8) cm. The configurations are stable for reflector height in the (5.57, 6.52 cm) range (Figure 12). As also observed previously in Section 10.1, the first plot in Figure 12 seems to suggest that there is perhaps another range of reflector heights ($h < 4$ cm) for which the configuration

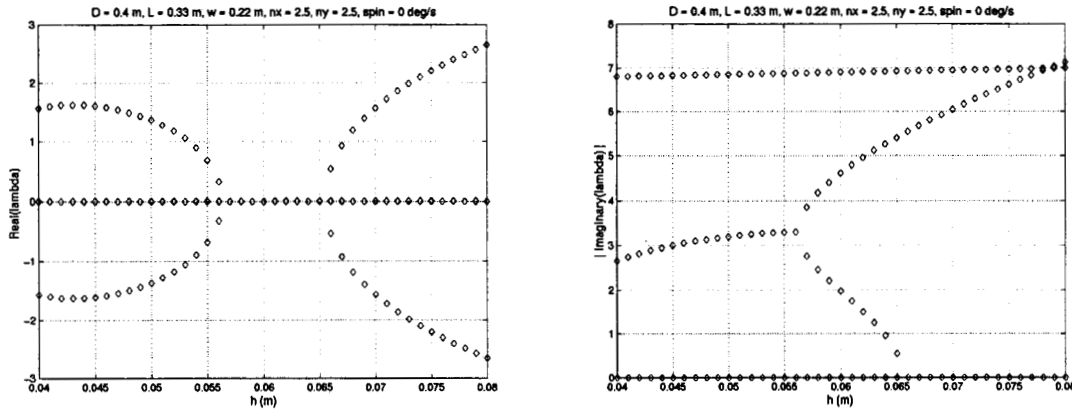


Figure 12. Variation in Neutral Stability with Reflector Height h

will be neutrally stable. Extending the h range to values below 4 cm the plot on the left in Figure 12 takes the appearance shown on the left in Figure 12a. Indeed a second, very narrow NS h range exists around $h = 3.5$ cm. The plot in the neighborhood of $h = 0.035$ m has been magnified on the right in Figure 12b, where the second NS h range is seen to be (3.43, 3.47) cm. It is noteworthy that a smaller height results in a flatter reflector, which tends to lose translational stability, while an increase in height also destroys stability by reducing the incidence angle (the angle between the incident radiation and the

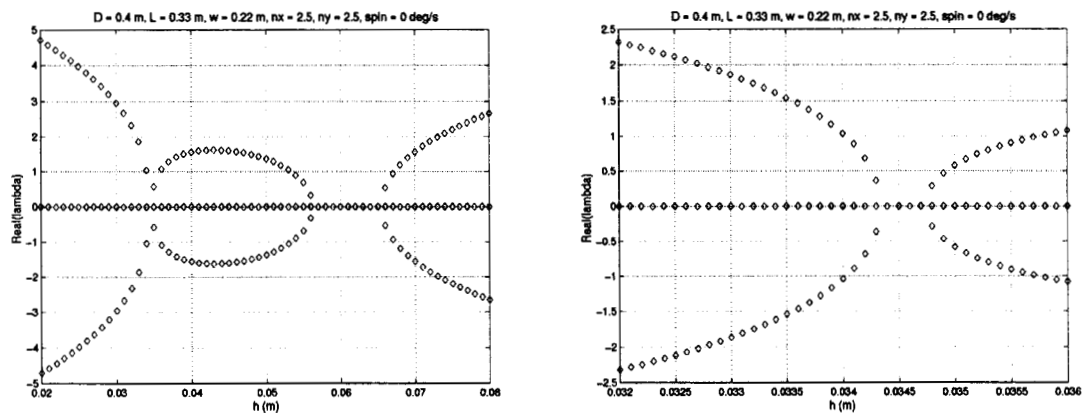


Figure 12b. The Second NS Range of Reflector Heights

surface normal) on the outboard elements, defeating the benefits of a favorable beam flux gradient. The restoring force decreases with increasing height until a critical value is reached beyond which the configurations are not stable.

10.6 Variation in Spin Rate, Ω : $0 \leq \Omega$

Vehicle spin rate is an important parameter which can be used to stabilize an otherwise unstable configuration. It certainly helps to “stiffen” the vehicle in attitude. It is well known that a spin about an axis of maximum inertia is stable in attitude. Actually, a spin about an intermediate inertia axis is unstable for a rigid vehicle. Energy dissipation, however, would make a spinning vehicle acquire a steady state in which it is spinning about the maximum inertia axis. Note that so far we have ignored natural damping in our analysis. But, however small it may be, it will be present in real vehicles.

The aforementioned characteristics of passive stability of a spinning vehicle hold only when there are no external torque influences on the vehicle, which is not the case here. These inferences are applicable only when the power is turned off in our case. An assessment of the vehicle’s passive spin stability properties in the presence of the radiation field under consideration will require a detailed analysis, beyond the scope of the analysis presented here. Note that the axis we would like to spin about is the z_b axis or the symmetry axis of the vehicle, which incidentally is not the maximum inertia axis for the vehicle configurations under consideration (it is the minimum inertia axis). We shall assume that a spin about an axis of minimum inertia will not pose a problem here (further analysis and experiments will be needed to support this assumption). Note however that if it proves to be a concern, the vehicle configuration can be modified to make the z_b axis the maximum inertia axis of the vehicle. This is achieved by simply removing or shortening the mast substructure. The mast was introduced as a means to induce passive attitude stability, which, for a spinning vehicle, will be derived from spin stiffening. We will not consider such configurations here and proceed with the assumption that a spin about an axis of minimum inertia will not pose a problem.

The parameter set chosen for illustration here is as follows: $\mathcal{P}^* = \{D = 0.4 \text{ m}, L = 0.33 \text{ m}, w = 0.22 \text{ m}, n_x = n_y = 2.5, h = 6 \text{ cm}, \Omega\}$. Spin rate is varied from $0 \rightarrow 1000^\circ/\text{s}$. The related eigenvalue plots appear below in Figure 13. It is interesting to note that the vehicle which is NS at 0 spin, becomes unstable for spin rates in the $67^\circ/\text{s} \rightarrow 450^\circ/\text{s}$ range. The hopping mode frequency remains invariant as spin rate is increased (expected) and the frequencies of two of the remaining four modes exhibit a strong, near-linear dependence on the vehicle spin rate at large spin rates.

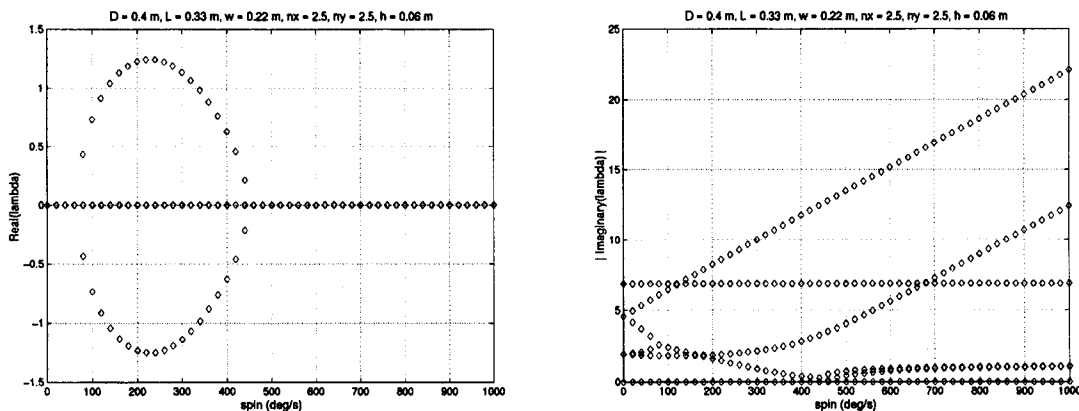


Figure 13. Variation in Neutral Stability with Vehicle Spin Rate

11. Domains of Stability

Once a neutrally stable configuration has been determined, it is natural to address the question of domain of stability, i.e. for what range of initial conditions or perturbations from the equilibrium state do the ensuing motions remain bounded? A limited perturbation set is considered here. Recall that the equilibrium noted in Section 9 places the vehicle directly above the power source with its attitude aligned with the inertial frame. The perturbations considered here move the vehicle laterally while keeping all other elements of state \bar{x} fixed. Numerical integration of equations of motion is carried out at each perturbed initial condition \bar{x} . Computation of the stability domain is a very time consuming process where a number of simulations must be run. A number of simulations were carried out to determine that a simulation duration of about 100 seconds is perhaps enough for each initial condition (i.e. if the vehicle does not remain atop the beam or “fall-over” in 100 seconds, it will never do so and motions will remain bounded forever).

Domain of stability is the set of all vehicle initial conditions, which are perturbations of \bar{x} in the X_I - Y_I plane, such that the ensuing vehicle motions remain bounded. Put another way, if the vehicle motions starting at $\bar{x} = \{x, y, -d, 0, 0, 0, 1, 0, 0, 0, 0, \Omega\}$ remain bounded then the set (x, y) belongs to the domain of stability. The domain of stability is therefore a region in the inertial X_I - Y_I plane. Note that the z coordinate ($z = -d$) is chosen so that the parameter D once again specifies the reflector-source separation (see the discussion in Section 9). Also, the vehicle is allowed to have a z -axis spin (Ω) in the perturbed state. We intend to vary it to show its effects on the domain of stability.

The domain of stability is expected to a contiguous region. It is also expected to have symmetry, i.e. once a quadrant of the domain has been determined, other quadrants are obtained as reflections about the X_I or the Y_I axis. The initial search for a point on the boundary starts in the X_I direction until a point on the boundary $(x^*, 0)$ has been found. The search then considers a neighboring point $(x^* + \delta x, \delta y)$. If this initial condition does not result in a bounded motion behavior, the x coordinate is decremented in steps of δx , else it is incremented in steps of δx . This process of incrementing or decrementing the x coordinate, in steps of δx , at the fixed y location is carried out until the domain boundary is crossed. The y coordinate is incremented in steps of δy until the search ends on the Y_I axis, i.e. at the coordinate $(0, y^*)$. The search steps $\delta x, \delta y$ are user-defined parameters.

The domain of stability is, like stability itself, a function of vehicle shape, mass, and beam distribution parameters. We consider a few parameter variations next. The first variation considers the parameter set: $\mathcal{P}^* = \{D = 0.4 \text{ m}, L = 0.33 \text{ m}, w = 0.22 \text{ m}, n_x = n_y = n, h = 0.06 \text{ m}, \Omega\}$. A circular cone reflector is assumed once again. Five sets of variations are considered $(n, \Omega) = (2.3, 0^\circ/\text{s}), (2.5, 0^\circ/\text{s}), (2.7, 0^\circ/\text{s}), (2.9, 0^\circ/\text{s}), (2.3, 1000^\circ/\text{s})$. The stability boundaries are shown in Figure 15. The field and the reflector are both symmetric here. The domain is therefore, expectedly, a circular disc in the XY plane. Note that the domain, although it (expectedly) gets bigger for a spinning vehicle does not change appreciably. A greater change is noticed when the power gradient is made sharper (larger n), in which case the domain is seen to shrink.

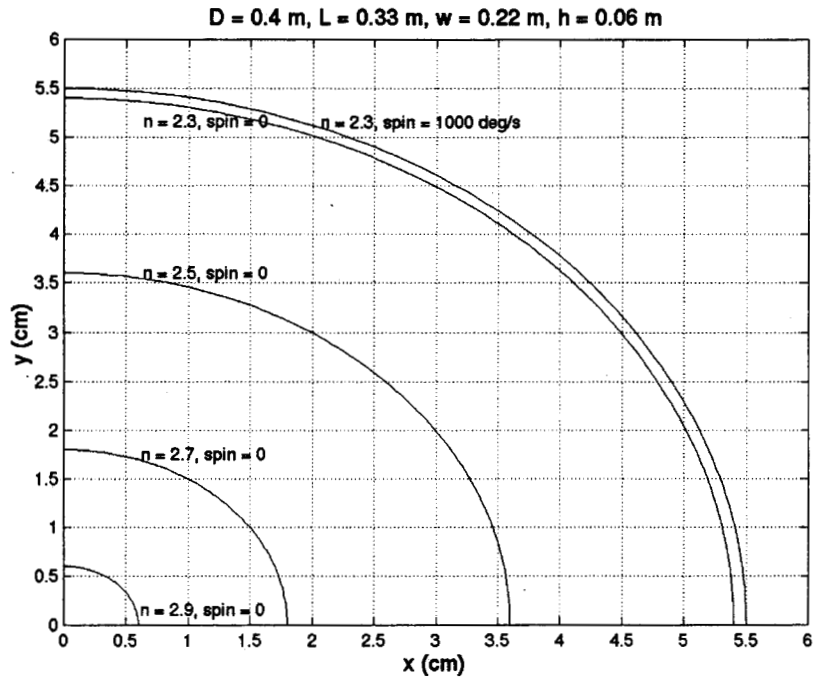


Figure 15. Stability Domain Boundaries when n is Varied

Next parameter variation considers the nominal set: $\mathcal{P}^* = \{D = 0.4 \text{ m}, L = 0.33 \text{ m}, w = 0.22 \text{ m}, n_x = n_y = 2.3, h, \Omega = 0^\circ/\text{s}\}$. Two values of h are considered: 6.2 cm and 5.8 cm. Related boundaries are depicted in Figure 16. A smaller domain exists for a shallower reflector.

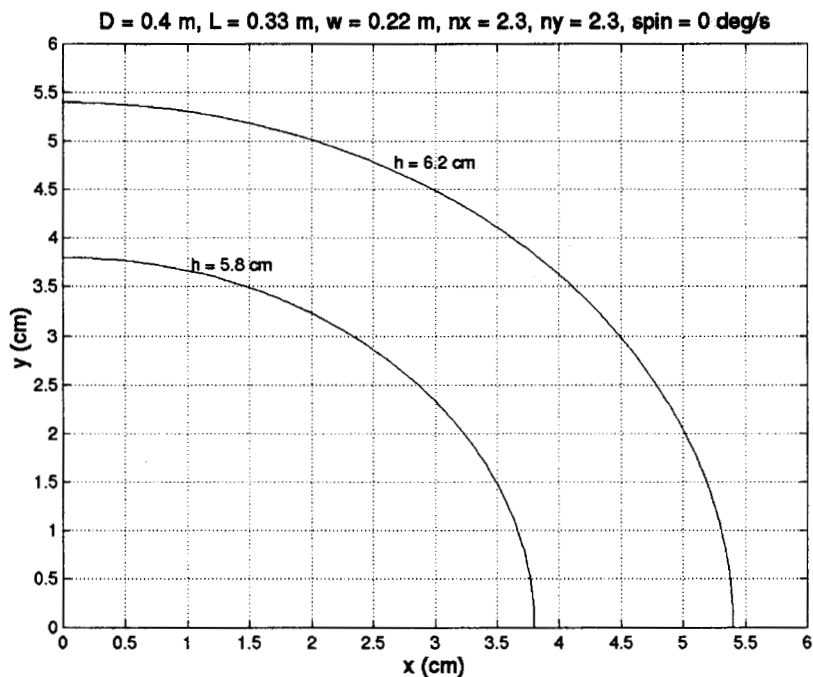


Figure 16. Stability Domain Boundaries when Reflector Height h is Varied

12. Description of the Simulation Model and Environment

A vehicle dynamics model was created using the commercially available software package SD/FAST, which facilitates dynamics modeling of a system of hinge-connected rigid bodies. The system is modeled as a system of two rigid bodies which are connected by a 2-DOF rotational hinge. The two rigid bodies will be referred to as the reflector-substructure and the mast-substructure. The hinge, whose intent will soon become apparent, allow relative rotations to take place between the mast-substructure and the reflector-substructure.

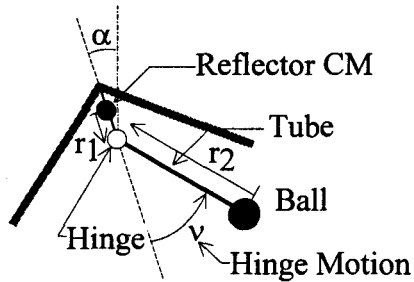


Figure 17. The 2-Body System

The hinge can be locked so that no relative motion is allowed. A planar depiction of this arrangement is shown in Figure 17. Vector r_1 locates the hinge with respect to the reflector CM and the vector r_2 locates it relative to the spherical Lead ball on the mast (see Section 6 for mast model assumptions). A tubular structure, similar to the tube on the mast, is assumed on the reflector side. It defines the physical connection between the hinge and the reflector CM.

The dynamics simulation, a collection of functions written in the C language, can be run in three "modes". At the start of a program execution, the user is prompted to select one of the following three options.

```
Enter execution mode:
  [1] = Time Simulation
  [2] = Stability Boundary Computation
  [3] = Linearization (for Eigenanalysis)
```

The meaning of each of these is obvious. Selection of mode [1] allows the user to run a time simulation, [2] is used to numerically compute the domain of stability and [3] is used to evaluate the Jacobian A (eqn.15), whose eigenvalues must be numerically evaluated in order to determine neutral stability in the neighborhood of the chosen state. Three "parameter" files: param_inputs, param_sim, and param_ic are read by the program.

12.1. Fields in param_inputs

The first group in this set of inputs allows the user to enter the reflector shape and density data, which are: the mass per unit area in units of gm/m^2 , the base dimensions a and b in meters, number of discrete elements / half-span (needed for the evaluation of (10), (11)), and the shape coefficients c_j , $j = 0, 1, 2, 3, 4$ (eqn.(1)).

```
Reflector Data:
  Mass / Area      (gm/m2)    = 5
  Half-Span X,Y    (m)        = 1.1e-01 1.1e-01
  Number Of X,Y Elements = 25 25
  Shape Coeff 0    = 0
  Shape Coeff 1    = -.06
  Shape Coeff 2    = 0
  Shape Coeff 3    = 0
  Shape Coeff 4    = 0
```

The next group of parameter in `param_inputs` specifies the mast mass properties and hinge location. Recall that a 2 degrees-of-freedom hinge is located at the point where the mast is attached to the reflector (Figure 17). The user specifies the following:

```

Mast Data:
vector r1          (m)      = 0 0 -0.33
vector r2          (m)      = 0 0 0
tube density       (kg/m3) = 4510.0
tube radius        (m)      = 0.50e-3
tube thickness     (m)      = 0.20e-3
ball density       (kg/m3) = 11300.0
ball radius        (m)      = 5.00e-3

```

Note that the location of the hinge is required as well as the size and density parameters related to the mast elements (the tube and the ball). In the specifications noted above, the hinge is co-located with the ball, i.e. $r_2 = (0, 0, 0)$ m. A tube element is missing from the mast side, but it is present on the reflector side, and the hinge is located 33 cm away from the reflector CM. Also note that the density values noted above are consistent with a Titanium tube and a Lead ball.

The next group of parameters specifies the properties of the relative articulation between the mast-substructure and the reflector-substructure. The location of the hinge was specified in the previous group of specifications. The hinge has 2 degrees of freedom. The articulation of each can be specified independently. It is possible to disable the articulation by setting the `Prescribed_Motion_Flag` to 1 (0 means that hinge motions are allowed). Subsequent fields are ignored for a 1 value of this flag (each axis). In case articulation is allowed, it is possible to place a rotational spring and a dashpot about each articulation axis. The stiffness and damping of these passive devices is specified next. Actual values used (which are scaled using mast, and reflector inertia) by the simulation is echoed at the start of the simulation. Note that in the following specification, articulations about both axes are disabled and the hinge degrees of freedom are parallel to the vehicle x and y axes.

```

Hinge Joint Properties:
Prescribed Motion Flag = 1 1
Joint1Orientation      = 1 0 0
Joint2Orientation      = 0 1 0
Stiffness              (Hz) = .008 .008
Damping                = .006 .006

```

The next group allows the user to input appropriate gravity vector (G) in inertial frame.

```

Gravity Field:
Accel Vector          (m/s2) = 0 0 -9.807

```

The following allows the user to specify the power source location with respect to the reflector CM in inertial coordinates and the beam shape by choosing appropriate values for the power indices n_x and n_y .

```

Beam Data:
ReflectorCM2Source   (m)      = 0 0 -.4
Power Index          (x, y)   = 2.5 2.5

```

12.2. Fields in param_sim

The simulation control parameters are specified here. These are used for execution modes [1] and [2]. A fixed-step RK-4 integration method is used here. The user must specify the numerical integration step size, simulation end time and the time resolution of the quantities output by the simulation (0.1 second in the following).

```
Integration Step Size (sec): 0.005
Simulation Final Time (sec): 100
Simulation Output dt (sec): 0.1
```

12.3. Fields in param_ic

The inputs noted here allow the user to control simulation initial conditions for time-simulation and linearization, and search step size for computation of domain of stability. The first group sets the desired elements of vehicle initial position, velocity, attitude, and angular rate. The dynamics is linearized about the state specified here. `Position` and `Velocity` fields specify the reflector-substructure CM location and velocity in inertial frame. `Attitude` field is the specification of Euler angles for a 3-2-1 Euler sequence to locate the body frame in inertial coordinates, and `Angular_Rate` is the reflector angular rate. In the following the vehicle is at rest, directly above the power source, and spinning about its z axis at a rate of 2000°/s.

```
Inputs for linearization:
Position (m) = 0 0 0
Velocity (m/s) = 0 0 0
Attitude[x,y,z] (deg) = 0 0 0
Angular Rate (deg/s) = 0 0 2000
```

The following group allows the user to set the vehicle initial conditions for a time simulation (elements of state, except the x and y coordinates of reflector position, for computing the domain of stability boundary are also taken from this group).

```
Reflector Initial State:
Position (m) = 0.05 0.03 0
Velocity (m/s) = 0 0 0
Attitude[x,y,z] (deg) = 0 0 0
Angular Rate (deg/s) = 0 0 2200

Pendulum Angles Initial State:
Hinge (deg) = 0 0
Hinge Rates (deg/s) = 0 0
```

The last group sets the parameters related to the computation of the domain of stability. The user can select the initial values (x,y coordinates of the reflector-substructure CM in inertial coordinates) and the size of the search grid (parameters δx , δy of Section 11). As noted earlier, all other state values are taken from the group specified above.

```
Inputs for stability analysis:
Initial value (x,y) = 0.055 0.0
Increment (x,y) = 0.002 0.002
```

12.4. Simulation Outputs

Execution mode [1]: Files `pos_data` and `vel_data` are created. The first column in each is the time variable. The `pos_data` file contains columns of vehicle CM location (columns 2, 3, 4, in meters in inertial coordinates), vehicle attitude quaternion (next four columns), and pendulum deflection angles (the last two columns, in radians). The file `vel_data` contains time-tagged values of reflector CM velocity (three columns, in meters/sec in inertial coordinates), vehicle angular rate (three columns, in radians/sec in body coordinates), pendulum deflection rates (two columns, in radians/sec), and beam flux at the reflector CM location. Note that the pendulum deflection angles and rates must be zero or very close to it when no articulation is allowed at the hinge. The `simulation_output_dt` field of `param_sim` controls the time resolution in these files.

Execution mode [2]: A `bnd_data.m` file is created. This file contains the (x^*, y^*) coordinates of the boundary of the domain of stability as the matrix `bndry`.

Execution mode [3]: The file `eig_data.m` containing elements of the Jacobian A is created. Evaluation of eigenvalues will require loading this file in MATLAB and invocation of the eigenvalue calculation function (e.g. `eig(A)`).

13. Representative Time-Simulations

Some representative time histories of vehicle states are presented next. We will consider the parameter set: $\mathcal{P}^* = \{D = 0.4 \text{ m}, L = 0.33 \text{ m}, w = 0.22 \text{ m}, n_x = n_y = 2.3, h = 0.06 \text{ m}, \Omega = 0 \text{ }^\circ/\text{s}\}$. A circular base, conical reflector of 6 cm height and 22 cm span is therefore used. The reflector CM is located 40 cm above the circular power source (power index = 2.5). Total vehicle mass is 7.07 gm, of which only 0.22 gm belong to the reflector structure. Nearly 663 MW of power is needed to have the vehicle levitate approximately 40 cm away from the source. The reflector CM is moved off center to a location (4, 2) cm in inertial XY coordinates. The ensuing motions are shown in Figure 18. The three plots on the left show, from top to bottom, the reflector CM motions in the inertial YZ plane, inertial XZ plane, and the inertial XY plane (the “top” view of the motion). The top plot in the middle column depicts vehicle attitude time history. Attitude motions of the order of 1.2° are realized here. The middle plot shows the change in vehicle CM translation coordinates as a function of time (@ $t = 0$ the vehicle CM Z-location = -0.3 m). The z motions do not exceed ± 1.5 cm in this case. The next plot depicts the vehicle velocity time history, which suggests that speeds were limited to 7 cm/s here. Finally the two plots at the bottom right depict the reflector shape projections onto the xy and xz body frames. Some of the relevant vehicle and power source data is also noted on the right. Note that while z_b axis is the vehicle minimum inertia axis, it is the reflector maximum inertia axis. Total reflector surface area is approximately 434 cm^2 . The `param_inputs` file in this case reads as follows:

```
Reflector Data:
Mass / Area          (gm/m2)      = 5
Half-Span X,Y       (m)          = 1.1e-01 1.1e-01
Number Of X,Y Elements = 25 25
Shape Coeff 0       = 0
Shape Coeff 1       = -.06
```

Shape Coeff 2 = 0
 Shape Coeff 3 = 0
 Shape Coeff 4 = 0

Mast Data:
 vector r1 (m) = 0 0 -0.33
 vector r2 (m) = 0 0 0
 tube density (kg/m3) = 4510.0
 tube radius (m) = 0.50e-3
 tube thickness (m) = 0.20e-3
 ball density (kg/m3) = 11300.0
 ball radius (m) = 5.00e-3

Hinge Joint Properties:
 Prescribed Motion Flag = 1 1
 Joint1Orientation = 1 0 0
 Joint2Orientation = 0 1 0
 Stiffness (Hz) = .008 .008
 Damping = .006 .006

Gravity Field:
 Accel Vector (m/s2) = 0 0 -9.807

Beam Data:
 ReflectorCM2Source (m) = 0 0 -0.4
 Power Index (x,y) = 2.3 2.3

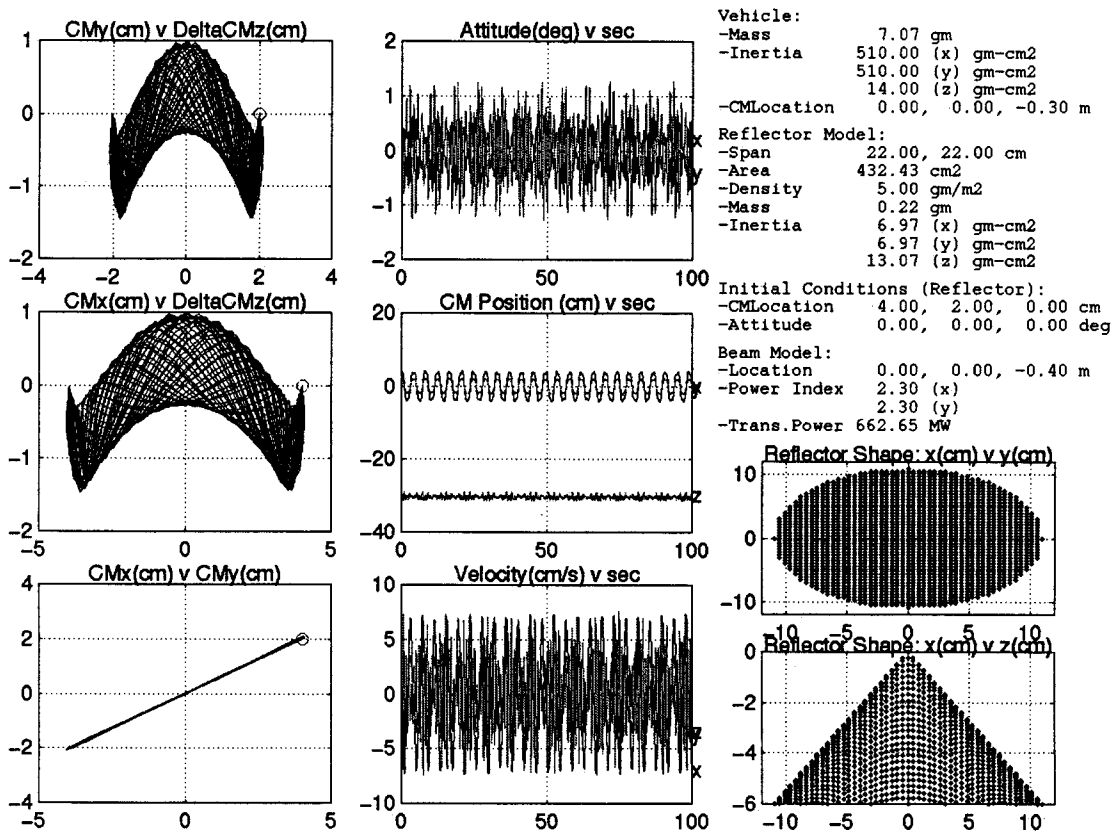


Figure 18. Vehicle Motions for a Neutrally-Stable Vehicle

14. Realization of Passive Damping

The reflector-mast arrangement possesses insignificant amounts of natural damping, which is derived primarily from heat-dissipation through internal motions in the reflector structure. Presence of passive damping is a very desirable attribute which can possibly decay and limit overall motions of the vehicle. It is possible, in principle, to inject passive damping in the system by allowing articulation or relative motion at the point where the mast substructure is attached to the reflector substructure and placing a viscous dashpot (a rotational dashpot) at the point of articulation. A rotational spring will also be needed so that the relative motions between the mast substructure and the reflector

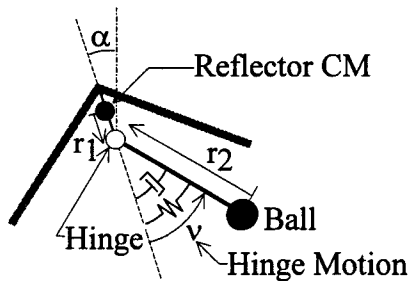


Figure 19. A Damped Beam-Rider

substructure, henceforth referred to as the hinge motions, remain zero-mean. The arrangement will, in general, dissipate energy through heat (heating of the viscous element). Figure 19 depicts such an arrangement for planar motions (the generalization to the general three-dimensional case is straightforward). Angle α is the vehicle attitude (compare with Figure 1) and, an additional degree-of-freedom, the angle ν denotes the hinge deflection (there are two such variables: one in-plane and the other out of plane). Also note that in

general there can be an offset between the hinge location and the reflector CM (vector r_1). The result is a vehicle which now possesses 8 DOF. Note that, in general, one should not expect such an arrangement to be stable or damped for all r_1 and r_2 values. These vectors locate the 2-DOF hinge with respect to the reflector CM and the ball on the mast substructure. Such an arrangement can in fact destabilize an otherwise neutrally-stable vehicle. The utility of such an arrangement is to impart damping to vehicle natural motions. The key therefore is to determine desirable hinge locations and appropriate damping and stiffness values for the spring-dashpot arrangement. Furthermore, it is desirable to have an arrangement which would maximize hinge motions (so that damping may take place at a faster pace). In general, vehicle translation and attitude motions both contribute to hinge deflections. A desirable configuration from maximizing hinge motions standpoint requires that the hinge be placed near the mast CM (i.e. $|r_2| \ll |r_1|$). We present a time simulation of another configuration, which is NS with the hinge locked and also meets the multiple-reflection condition. A 34 cm diameter, 9 cm high reflector sitting atop a 33 cm mast, 40 cm away from the radiation source ($n_x = n_y = 2.5$) is used in this case. The `param_inputs` file in this case reads as follows (the hinge locked instance).

```
Reflector Data:
Mass / Area      (gm/m2)      = 5
Half-Span X,Y   (m)              = 1.7e-01 1.7e-01
Number Of X,Y Elements = 25 25
Shape Coeff 0   = 0
Shape Coeff 1   = -.09
Shape Coeff 2   = 0
Shape Coeff 3   = 0
Shape Coeff 4   = 0
```

```

Mast Data:
vector r1      (m)      = 0 0 -0.33
vector r2      (m)      = 0 0 0
tube density   (kg/m3)  = 4510.0
tube radius    (m)      = 0.50e-3
tube thickness (m)      = 0.20e-3
ball density   (kg/m3)  = 11300.0
ball radius    (m)      = 5.00e-3

```

```

Hinge Joint Properties:
Prescribed Motion Flag = 1 1          ← Hinge locked
Joint1Orientation      = 1 0 0
Joint2Orientation      = 0 1 0
Stiffness              (Hz) = .008 .008
Damping                = .006 .006

```

```

Gravity Field:
Accel Vector          (m/s2) = 0 0 -9.807

```

```

Beam Data:
ReflectorCM2Source (m) = 0 0 -.4
Power Index        (x,y) = 2.5 2.5

```

Motion eigenvalues were numerically determined to be (note that small numbers, i.e. numbers of the order of 10^{-16} have been expressed as exact zeros in the following):

```

0 (repeated 7 times)
0 ± 1.1646e+00i (repeated 2 times)
0 ± 3.1848e+00i (repeated 2 times)
0 ± 6.4547e+00i

```

In the case to be presented next, we “release” this lock. The param_inputs file in this case reads exactly as shown above except that the Prescribed_Motion_Flag fields are now 0, 0. The stiffness and damping values specified in this file are scaled by appropriate inertia values. The actual (physical) values used by the dynamics simulation are 2.368×10^{-7} Nm/rad of stiffness and 5.654×10^{-8} Nm/ rad/s of viscous damping. The system eigenvalues when the hinge articulation is allowed become:

```

0 (repeated 3 times)
-3.5576e-05 ± 1.1645e+00i (repeated 2 times)
-4.2908e-04 ± 3.1857e+00i (repeated 2 times)
-4.7772e-01 ± 1.9432e+00i (repeated 2 times)
0 ± 6.4547e+00i

```

Note that there is no change in the hopping mode frequency (expected) but the other eigenvalues (the second and the third sets for the undamped case) which were located on the imaginary axis now have a small negative real part associated with them, indicating that these modes will have some damping associated with them. The other eigenvalues are related to the hinge modes. The time histories for this case are shown in Figure 20. The initial conditions of Figure 18 are employed. The data time resolution in these plots is 1 second (0.1 second in Figure 18). Nearly 310 MW are needed to support the vehicle. The fact that motions are damped is not immediately obvious. Motions over a longer time scale must be observed in order for the presence of (small) damping to become obvious. The two damping time constants are 28113 seconds ($= 1.0/3.5576 \times 10^{-5}$) and 2330 seconds ($= 1.0/4.2908 \times 10^{-4}$), meaning that it will take, in the worst case,

approximately 20000 seconds for motion amplitudes to reduce to about half their initial values.

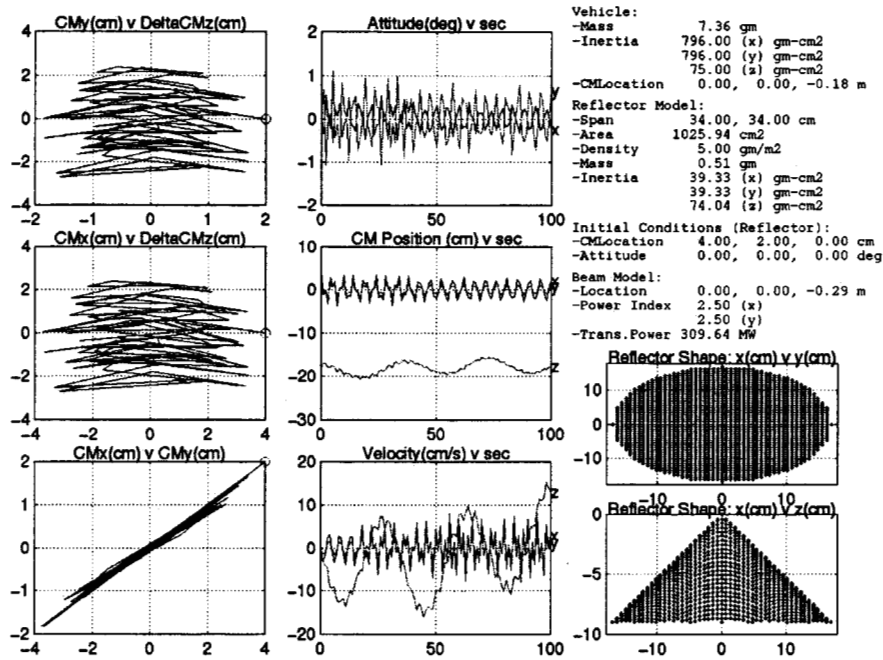


Figure 20. Vehicle Motions for a Damped Vehicle Configuration

A simulation lasting 4560 seconds was carried out next. The position and attitude variations for the first 100 seconds and the last 100 seconds of the 4560 seconds simulation are shown side by side in Figure 20a. Plotting scales are identical for the two time segments shown here. Presence of damping is clearly apparent from these plots.

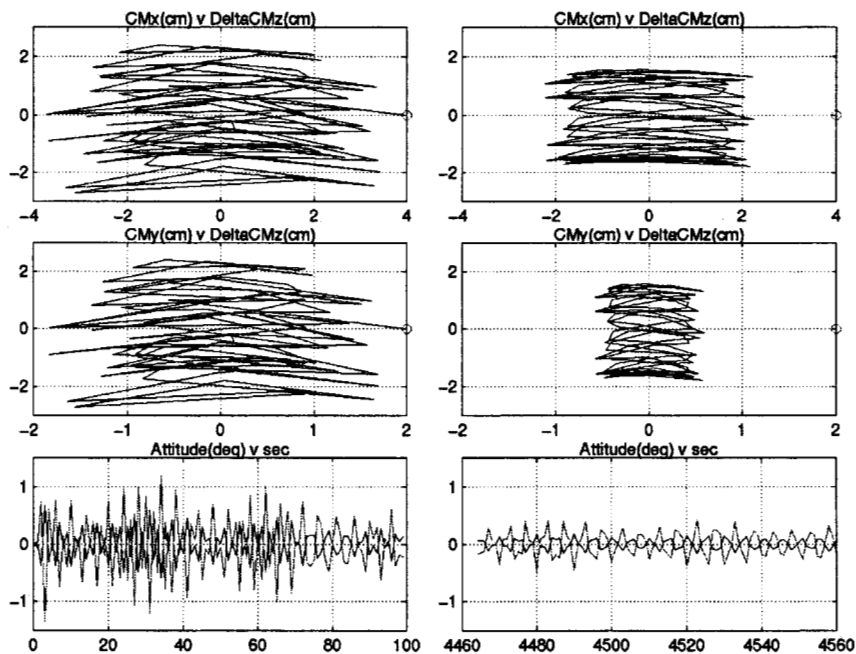


Figure 20a. Damping of Motions for a Damped Vehicle Configuration

The only residual vehicle motion, after other motions have completely damped out will be related to the hopping mode which is unaffected by damping mechanism employed here. In the steady state therefore, the vehicle will be located directly above the beam source and moving up and down with a peak-to-peak amplitude of approximately 3 cm. The related hinge deflections are shown below in Figure 21 (there are two plots here, one for each hinge axis). Again, the first 100 seconds (left) and the last 100 seconds (right)

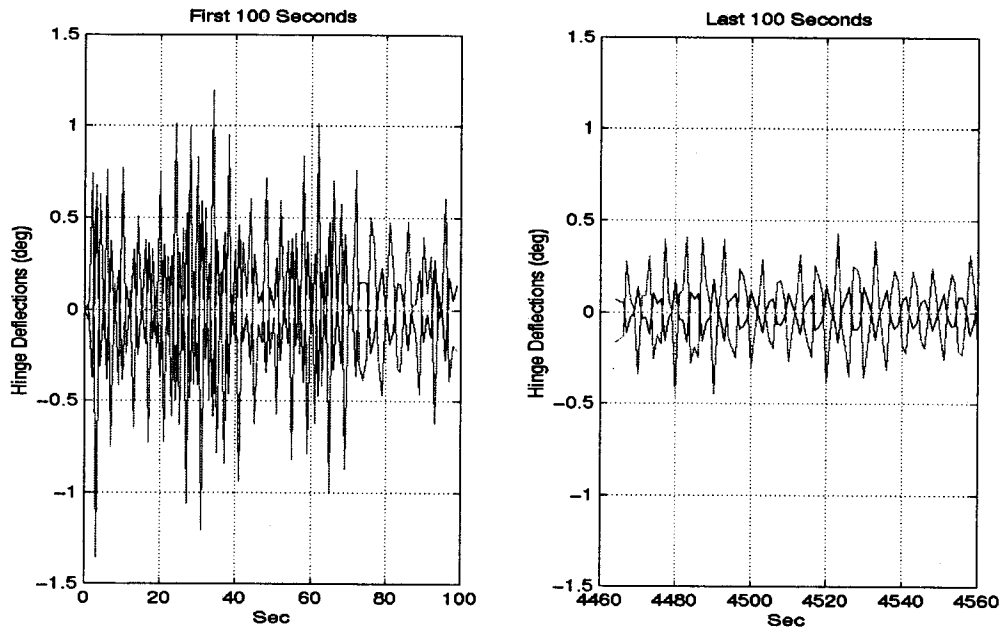


Figure 21. Hinge Deflections Time Histories : The First and The Last 100 Seconds

time slices are shown here. These motions are obviously damped and will also approach a null value in the steady state. Note that passive damping will take place for as long as the deflections are not zero, and, in the steady state, only the hopping mode will be a participant. It is a matter of simple “extrapolation” to design a mechanism which can also damp out the hopping mode motion. One might do so by placing a linear hinge or a sliding joint along the mast axis. Such a joint may be located on either side of the rotational hinge. How such a configuration might look like is shown in Figure 22 (sliding joint in on the ball side). Motions induced by hopping mode will naturally cause relative

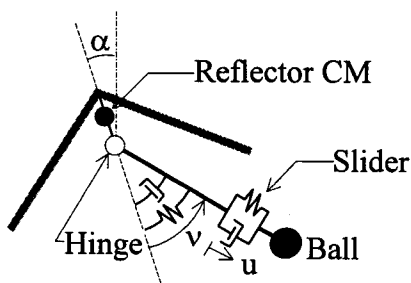


Figure 22. A “Completely” Damped Beam-Rider

motions (the coordinate u in Figure 22) across the linear joint. It will be possible therefore to damp the hopping mode by placing a linear spring and a linear dashpot along this sliding articulation. This possible arrangement is not investigated here but one might do so in future extensions of this work. Such a craft configuration will have a total of 9 degrees-of-freedom: 6 for the rigid reflector, one for each of the two rotational degrees of freedom of the rotational hinge and one for the linear hinge along the mast axis.

15. Conclusions and Recommendations For Future Work

The modeling, stability analysis, and simulation work related to a microwave sail vehicle is considered here. The key questions addressed in this report are:

- 1) For what shapes is it possible achieve a bounded motion behavior of the vehicle?
- 2) For neutrally-stable vehicles, what are the limits on vehicle lateral perturbations for which the ensuing motions will remain bounded?.
- 3) How is it possible to impart passive damping to the vehicle?
- 4) What are effects of spin on vehicle stability and dynamic characteristics?

To our knowledge, none of the published literature has ever attempted to address these issues for microwave sail vehicles. We have identified a shape which we have shown to possess neutral dynamic stability. Many more sail shapes remain unexplored, however, and this is one area where significant strides can be made by, both, ruling in or out certain reflector shapes.

We have attempted to characterize vehicle domain of stability as the set of all lateral excursions for which the ensuing motions will remain bounded. This particular aspect of the analysis is extremely time consuming and, again, the results offered here begin to shed some light on what this domain looks like. This part of the analysis is perhaps the least complete. Significant additional effort will be required to completely characterize these regions as a function of all vehicle shape and environment parameters.

Perhaps one of the most important contributions of this work is the identification of mechanisms which allow some passive damping. Although the amount of damping introduced by the mechanism chosen here appears to be very little, a range of hinge locations, spring-dashpot values must be considered to optimize the damping achievable with passive mechanisms presented here. This optimization was not carried out here, and additional work is also needed in this area.

The analysis/simulation results presented here make the assumption that the incident radiation is reflected only once by the reflector structure. The absence of multiple reflections is the key assumption in the analysis. In order to allow consideration of a greater variety of reflector shapes, it will be important to model these effects.

The effects of spin on vehicle stability and dynamics are also not fully explored here. It is an important dynamic attribute which can be made full use of in a number of ways. Two obvious spin-induced benefits are: stabilization of a configuration which is unstable when not spinning, and a possible enlargement of the domain of stability. It is noted that spin-stability in the radiation fields under consideration might require the spin axis to be the axis of maximum inertia. Passive spin-stability of a mast-less vehicle configurations will therefore require further examination.

To conclude, the following specific directions need further exploration:

- 1) Accommodation of multiple internal reflections,
- 2) a complete characterization of "domain of stability",

- 3) investigation of reflector shapes other than cones which may be neutrally stable,
- 4) investigation of mast-less configurations which might be required for spin stabilization,
- 5) investigation into how the hinge location and hinge stiffness and damping effects damping,
- 6) investigation of the “completely” damped configuration like the one proposed in Figure 22, and
- 7) investigation of spin-up dynamics which might resonate or excite some of the vehicle natural motions, in particular the pendulum-yoyo modes.

16. References

1. Valitov, R.A., Kurush, V.D., and Orlov, V.G., “ An experiment in the direct conversion of an electromagnetic field into mechanical energy,” Soviet Physics – Technical Physics, 6(12), June 1962, 1068-1070.
2. Beam Power Density Model per R.M. Dickinson.